nature photonics

LETTERS

PUBLISHED ONLINE: 20 JANUARY 2013 | DOI: 10.1038/NPHOTON.2012.336

# *In vivo* three-photon microscopy of subcortical structures within an intact mouse brain

Nicholas G. Horton[1†], Ke Wang[1†], Demirhan Kobat[1†], Catharine G. Clark[2], Frank W. Wise[1], Chris B. Schaffer[2] and Chris Xu[1*]

**Two-photon fluorescence microscopy[1] enables scientists in various fields including neuroscience[2,3], embryology[4] and oncology[5] to visualize *in vivo* and *ex vivo* tissue morphology and physiology at a cellular level deep within scattering tissue. However, tissue scattering limits the maximum imaging depth of two-photon fluorescence microscopy to the cortical layer within mouse brain, and imaging subcortical structures currently requires the removal of overlying brain tissue[3] or the insertion of optical probes[6,7]. Here, we demonstrate non-invasive, high-resolution, *in vivo* imaging of subcortical structures within an intact mouse brain using three-photon fluorescence microscopy at a spectral excitation window of 1,700 nm. Vascular structures as well as red fluorescent protein-labelled neurons within the mouse hippocampus are imaged. The combination of the long excitation wavelength and the higher-order nonlinear excitation overcomes the limitations of two-photon fluorescence microscopy, enabling biological investigations to take place at a greater depth within tissue.**

Optical imaging plays a major role in both basic biological research and clinical diagnostics, providing a non-invasive or minimally invasive microscopic imaging capability with which to investigate biological tissue. However, optical image acquisition through significant depths of biological tissue presents a major scientific challenge because tissue is extremely heterogeneous, and the strong scattering of the various tissue components has historically restricted high-resolution optical imaging to thin sections or to superficial layers. The development of two-photon fluorescence microscopy (2PM) has significantly extended the penetration depth of high-resolution optical imaging, particularly for *in vivo* applications[8–12]. In the last 20 years, 2PM has enabled, in many fields for the first time, direct visualization of the normal behaviour of cells in their natural environment as well as their responses to systematic manipulations[3,13]. Two-photon excitation (2PE) of fluorescent molecules in tissue depends on the ability of sufficient excitation light to reach the focus of the objective unscattered (that is, ballistic excitation photons). The fundamental limitation on imaging depth for high-resolution 2PM is the signal-to-background ratio (SBR) of the excitation in scattering biological tissue[10,12] (for a derivation of SBR for 2PM see Supplementary Section S1), which for 2PM is typically between five and six effective attenuation lengths ($l_e$) below the tissue surface. For example, for 2PM in the mouse neocortex at 775 nm excitation ($l_e \approx 130$ μm), this depth limit is ~700 μm. An effective strategy for increasing the maximum imaging depth is to use longer excitation wavelengths to reduce the attenuation of the excitation light by tissue[11,12,14,15]. The optimum spectral window for excitation is determined by the trade-off between tissue scattering and absorption (typically dominated by water absorption in the near-infrared spectral region). Figure 1a shows the water absorption length ($l_a$)[16] and the calculated scattering length ($l_s$) of mouse brain tissue[10,12]. The combined effect of absorption and scattering is represented by $l_e$; that is, $l_e = (1/l_a + 1/l_s)^{-1}$. Figure 1a clearly shows that the optimum wavelength window in terms of tissue penetration is near 1,700 nm when both tissue scattering and absorption are considered.

A longer excitation wavelength alone cannot overcome the depth limit imposed by the SBR of 2PM. Three-photon fluorescence microscopy (3PM) was first demonstrated in the 1990s[17–19], mainly to extend the spectral range of the excitation source (for example, to access the transition band from 230 to 300 nm using a mode-locked Ti:sapphire laser). A significant advantage of 3PM that has largely been overlooked is that three-photon excitation (3PE) provides significant improvement in the overall excitation localization[17]. The fluorescence of 3PE falls off as $\sim 1/z^4$ (where $z$ is the distance from the focal plane), whereas the fluorescence of 2PE falls off as $\sim 1/z^2$. Therefore, 3PE dramatically reduces the out-of-focus background in regions far from the focal plane, improving the SBR by orders of magnitude when compared to 2PE (Supplementary Fig. S1). In addition, 3PE allows a wide variety of existing fluorescent dyes, fluorescent proteins and calcium indicators to be excited at the 1,700 nm spectral window (equivalent to a one-photon excitation of ~560 nm), eliminating the practical difficulty caused by the lack of fluorescent indicators at the 1,700 nm spectral excitation window for 2PE as well as the lack of good potential fluorescence detectors for the near-infrared wavelengths at which such dyes are likely to emit.

The amount of 3PE can be significantly increased by using a low-duty-cycle, high-pulse-energy excitation source[17], while still maintaining a low average power so as not to cause tissue heating[11]. We developed a novel high-pulse-energy source at 1,675 nm (Fig. 1c) using soliton self-frequency shift (SSFS)[20,21] in a photonic-crystal rod[22] pumped by a turnkey, energetic fibre laser at 1,550 nm (see Methods for details). The large mode-field area of the photonic-crystal rod enables the generation of high soliton pulse energy for 3PE. The measured output soliton energy of our source is 67 nJ at a repetition rate of 1 MHz, which is the highest soliton energy ever achieved through SSFS in a solid-core fibre. The measured soliton pulse width is 65 fs (Fig. 1b). SSFS not only shifts the wavelength to the desired 1,700 nm spectral window but also compresses the pulse width by a factor of 6, both essential for deep-tissue 3PM.

We performed *in vivo* imaging of mouse brain vasculature to demonstrate the capability of deep tissue imaging at 1,675 nm using 3PE (see Methods and Supplementary Fig. S2). The vasculature was labelled by a retro-orbital injection of dextran-coupled Texas Red dye (Invitrogen). We acquired a 1,400-μm-deep stack,

[1]School of Applied and Engineering Physics, Cornell University, Ithaca, New York 14853, USA, [2]Department of Biomedical Engineering, Cornell University, Ithaca, New York, 14853, USA; [†]These authors contributed equally to this work. *e-mail: chris.xu@cornell.edu

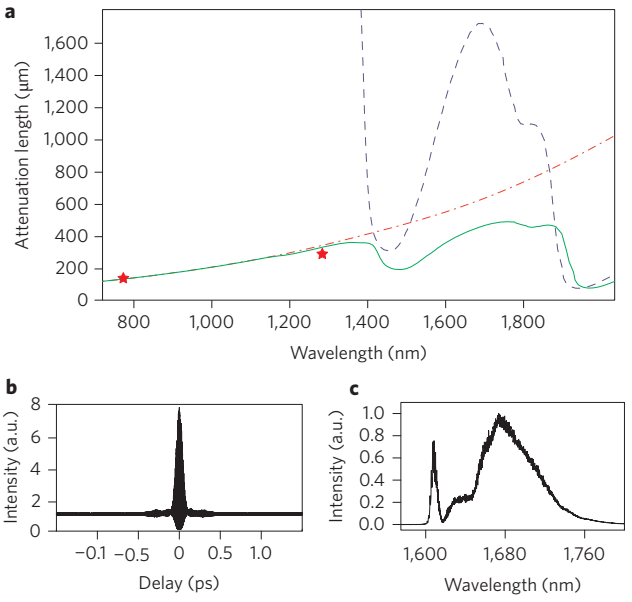


**Figure 1 | Wavelength-dependent attenuation length in brain tissue and measured laser characteristics. a**, Attenuation spectrum of a tissue model based on Mie scattering and water absorption, showing the absorption length of water ($l_a$, blue dashed line), the scattering length of mouse brain cortex ($l_s$, red dashed-dotted line), and the combined effective attenuation length ($l_e$, green solid line). The scattering length is calculated using Mie theory for a tissue-like phantom solution containing 1-μm-diameter polystyrene beads at a concentration of $5.4 \times 10^9$/ml, which resembles the scattering property of the cortex (grey matter). The red stars indicate the attenuation lengths reported for mouse cortex *in vivo* from previous work[11]. **b**,**c**, Measured second-order interferometric autocorrelation trace (**b**) and corresponding spectrum (**c**) of the 1,675 nm soliton generated in the photonic-crystal rod. The soliton energy, integrated from 1,617 nm, is 67 nJ.

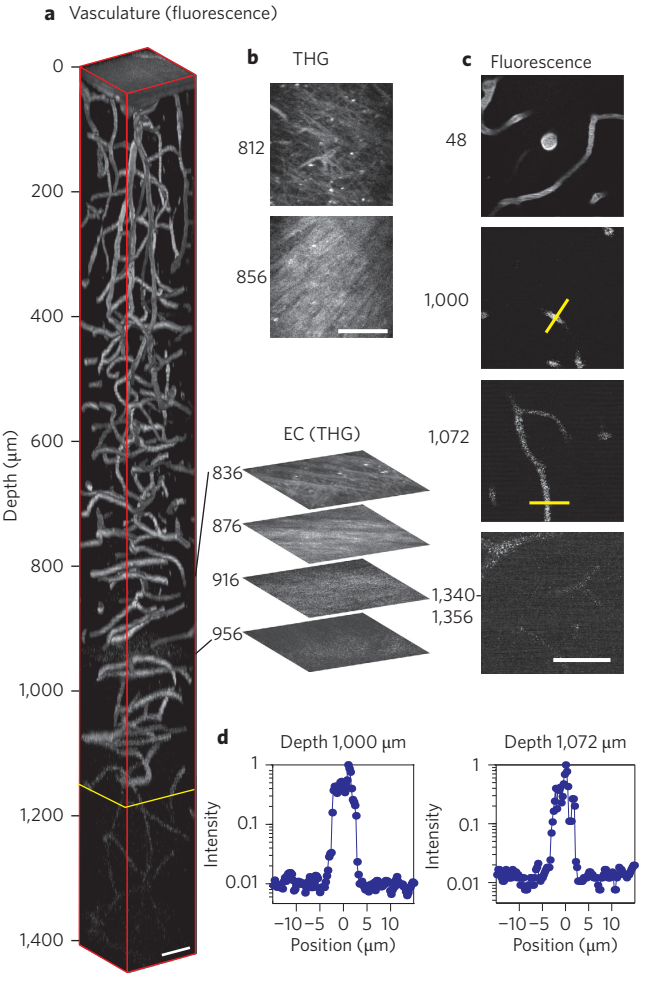


**Figure 2 | *In vivo* 3PM images of Texas-Red-dextran labelled mouse brain vasculature. a**, Three-dimensional reconstruction of 3PM images of the brain of an FVB/N mouse. The external capsule (EC) extends from ~840 to 956 μm below the surface of the brain. Frames deeper than 1,136 μm (yellow line) were normalized to the frame at 1,136 μm; all other frames were individually normalized. The expanded optical sections to the right are representative THG images from the external capsule region of the brain. **b**–**d**, Normalized *x*-*y* frames of the THG (**b**) and fluorescence signal (**c**) at various depths. The bottom frame in **c** is a *z*-projection of 20 μm. The fluorescence profiles of the lines across the vessels in the middle two panels in **c** are displayed in semi-logarithmic plots (**d**), which are used for SBR calculation. The background is calculated by averaging the intensity values between −15 and −5 μm and between 5 and 15 μm. All scale bars, 50 μm.

taken with 4 μm depth increments. Figure 2a shows the three-dimensional reconstruction of the data. By using the energetic excitation source we developed at ~1,700 nm, the average power required for 3PM at the surface of the brain in our experiments is ~3 mW, which is comparable to conventional 2PM. For optical sections within the first 0.8 mm of imaging depth, the excitation powers were adjusted so that approximately the same signal level, and thus the same signal-to-noise ratio (SNR), could be achieved at a constant frame time of 8 s (512 × 512 pixels per frame). Our excitation source was used at full power (22 mW at the sample surface) at depths beyond 0.8 mm, and the integration time was increased by a factor of 2.5 (20 s/frame). The myelinated axons in the external capsule (Fig. 2, EC, also known as 'white matter') produce a bright third harmonic generation (THG) signal[23–25] (Fig. 2a,b), which delineates the boundaries of the external capsule. Our images show that the external capsule begins ~840 μm below the surface of the brain. It is ~116 μm thick, and the CA1 region of the hippocampus begins ~956 μm below the surface of the brain. We were able to obtain high-resolution, high-contrast images of the blood vessels up to ~1,300 μm deep. From this data set, it is possible to determine a characteristic attenuation length (CAL) for 1,675 nm imaging in mouse brain tissue *in vivo*. For 3PE, we define the CAL as the depth at which the average fluorescence signal of the brightest 0.1% of pixels attenuates by $1/e^3$. Figure 4a shows the detected fluorescence signal as a function of imaging depth, from which the CALs are determined to be 365 μm between 56 μm and 840 μm (that is, the neocortex), 137 μm between 840 μm and 956 μm (that is, the external capsule), and 310 μm between 956 μm and 1,148 μm (that is, the CA1). In comparison, we had previously measured the CAL of the cortex to be 131 μm at 775 nm and 285 μm at 1,280 nm (refs 11,12). Furthermore, with 2PM at 1,280 nm, we had been unable to penetrate the external capsule using the same-aged animals at the same sagittal and coronal imaging position reported here[12].

We also performed quantitative SBR measurements at four depths between 1,000 and 1,135 μm (that is, within the CA1) and found the SBRs to range from 79 to 119. Two examples for depths of 1,000 μm and 1,072 μm are shown in Fig. 2c (middle panels) and Fig. 2d. The measured SBRs are lower than those predicted by theory (shown in Supplementary Fig. S1) due to the limited SNR of the images (signal level versus electronic noise floor) at these depths. Nonetheless, these SBR values are more than one order of magnitude higher than previous 2PM results at 1,280 nm at similar depths, but without the presence of the highly scattering external capsule[12].

We also imaged red fluorescent protein (RFP)-labelled neurons in a B6.Cg-Tg(Thy1-Brainbow1.0)HLich/J mouse[26] through a

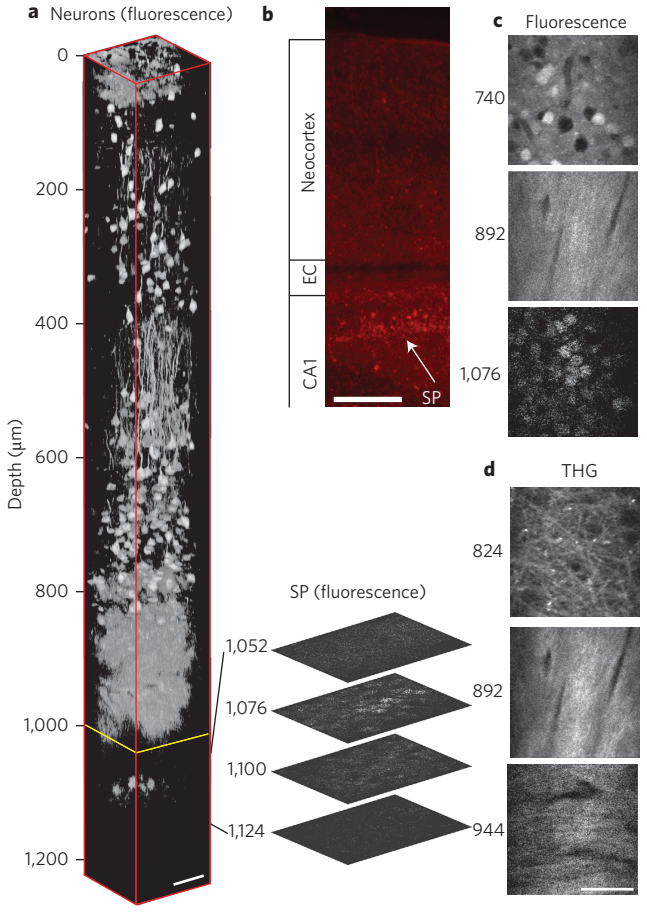


**Figure 3 | *In vivo* 3PM images of RFP-labelled neurons in mouse brain. a**, Three-dimensional reconstruction of 3PM images in the brain of a B6.Cg-Tg(Thy1-Brainbow1.0)HLich/J mouse, which contains RFP-labelled pyramidal neurons. Frames deeper than 992 μm (yellow line) were normalized to the frame at 1,076 μm (that is, the stratum pyramidale, SP). All other frames were individually normalized. The expanded optical sections to the right are representative fluorescence images of the stratum pyramidale. The external capsule extends from ~840 to 976 μm below the surface of the brain, and the stratum pyramidale extends from ~1,060 to 1,120 μm below the surface. Scale bar, 50 μm. **b**, Epifluorescence image of the coronal section of the mouse brain at approximately the same location as in **a**. The white arrow indicates the stratum pyramidale. Scale bar, 250 μm. **c**,**d**, Normalized *x*-*y* frames of the fluorescence (**c**) and THG (**d**) signal at various depths. Scale bar, 50 μm.

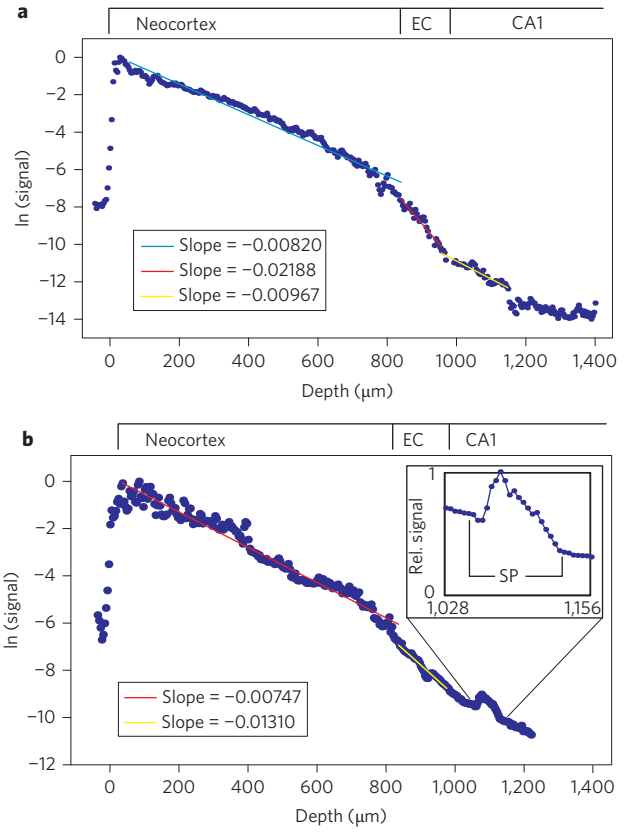


**Figure 4 | Fluorescence signal attenuation curves of *in vivo* experiments.** **a**,**b**, Semi-logarithmic plots of the fluorescence signal of the images in Fig. 2a (**a**) and Fig. 3a (**b**), normalized to the cubic of the laser power versus depth. EC, external capsule; SP, stratum pyramidale; CA1, CA1 region of the hippocampus.

cranial window (see Methods). The labelled cells include pyramidal neurons in the neocortex and the stratum pyramidale (SP), a dense layer of pyramidal neurons within the hippocampus. We acquired a 1,220 μm stack, taken with 4 μm depth increments. Imaging conditions were similar to those used in Fig. 2, except that our source was used at full power (22 mW) at 0.7 mm, and starting from 0.74 mm, the integration time was increased by a factor of 2 (16 s/frame). Beyond 0.9 mm, the integration time was increased again by a factor of 1.25 times (20 s/frame). Figure 3a shows the three-dimensional reconstructions of the data together with selected optical sections of the stratum pyramidale region. Bright fluorescence images with appearance nearly identical to THG images were obtained in the external capsule, indicating the expression of RFP in the axons there (Fig. 3c,d). Labelled neurons in the stratum pyramidale can be seen 1,060–1,120 μm below the surface of the brain (Fig. 3a,c). Visualization of this layer is clear evidence of direct imaging of the mouse hippocampus through an intact brain (Fig. 3b, Supplementary Fig. S3)[27]. Figure 4b shows the detected fluorescence signal as a function of imaging depth. From the slope of the line, we measured the CAL to be 401 μm between 36 μm and 840 μm (that is, the neocortex) and 229 μm between 840 μm and 976 μm (that is, the external capsule). The relative increase in signal at 1.1 mm is due to the cells in the stratum pyramidale. The fluorescence value is uneven within the hippocampus due to the layered distribution of the pyramidal neurons, which made a CAL calculation difficult in this region.

We measured the lateral brightness distribution of small features within the RFP-labelled mouse brain (Fig. 5a,b), which provides the upper bound of the lateral resolution. For example, at 644 μm and 844 μm depths within the mouse brain, the full-widths at half-maximum (FWHM) of the lateral brightness distributions are ~0.9 μm. The axial FWHM values are measured to be between 5.1 and 5.5 μm (average 5.3 μm) for five capillary blood vessels at depths between 817 and 948 μm below the surface of the brain (two examples are shown in Fig. 5c,d). Taking into account that the minimum diameter of the mouse capillary is ~3 μm (ref. 28), these values indicate that the axial resolution (FWHM) of our system is ~4.4 μm at these depths.

3PM at the new spectral window of 1,700 nm has potential as a powerful new tool for *in vivo*, high-resolution, deep-tissue imaging. By further improving the excitation source and microscope optics at 1,700 nm, we estimate that at least one order of magnitude improvement in frame rate can be achieved. In addition, by increasing the energy of the pump pulse and optimizing the photonic-crystal rod, a wavelength-tunable source that covers the entire 'low attenuation' spectral window from 1,650 to 1,850 nm can be obtained, which will further increase the number of accessible

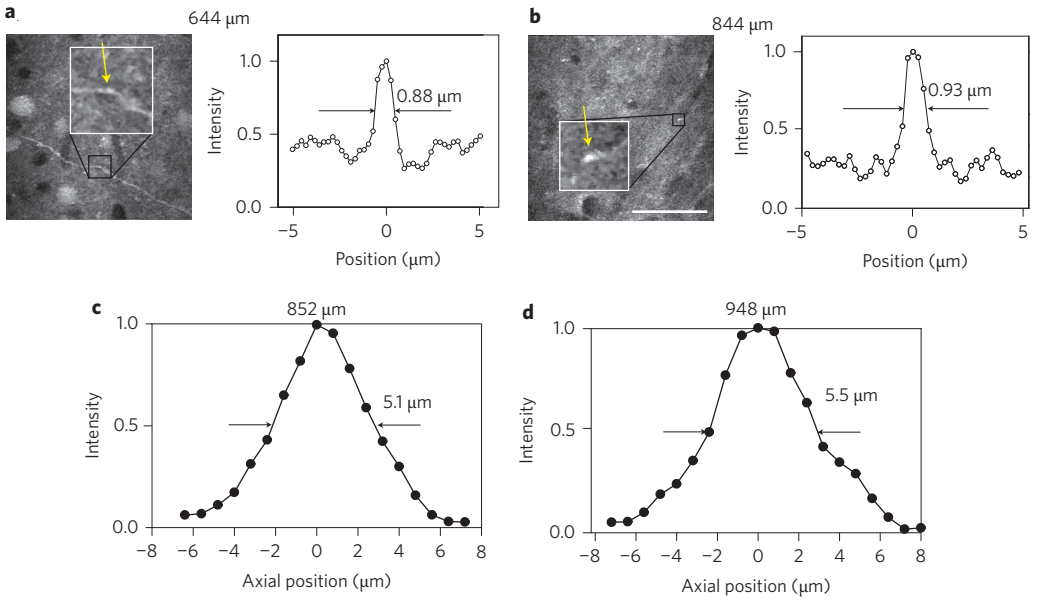


**Figure 5 | Resolution characterization of 3PM.** Intensity line profiles are used to characterize the lateral resolution. **a**,**b**, Sample *x*-*y* frames at 644 μm (**a**) and 844 μm (**b**) depths for the B6.Cg-Tg(Thy1-Brainbow1.0)HLich/J mouse. The line profile on the right is taken across a labelled neural process (indicated by yellow arrows in the images). Scale bar, 50 μm. **c**,**d**, Axial measurements of FVB/N mouse Texas-Red-stained capillary vessels at depths of 852 μm (**c**) and 948 μm (**d**).

fluorophores and fluorescent proteins for 3PE in the 1,700 nm spectral window.

## Methods

**Fibre-based excitation source.** The pump source for SSFS was a compact, turnkey, fibre-based femtosecond laser (FLCPA-01C, Calmar), delivering 360 fs, linearly polarized pulses with a repetition rate of 1 MHz at 1,550 nm. SSFS was performed in a commercially available, 36-cm-long, polarization-maintained (PM) photonic-crystal rod (DC-200-70-PM-Yb-ROD, NKT Photonics) with an effective mode area ($A_{eff}$) of 2,300 $\mu m^2$ at 1,550 nm. After collimation, a 1,600 nm long-pass filter (LPF, 1600ALP, Omega Optical) was used to filter out the residual pump. The soliton shifted to 1,675 nm at an input pulse energy of 500 nJ. The pulse width of the soliton was measured by performing second-order autocorrelation, and, assuming a $sech^2$ intensity profile, was found to be 65 fs (Fig. 1b). Owing to the dispersion of the microscope optics, the pulse width broadened to 79 fs after the objective. Pulse broadening due to propagation through brain tissue is mainly due to dispersion of water, because brain tissue is over 75% water. Our calculation showed that, after 2 mm of water (that is, the working distance of our water immersion objective lens), the 79 fs pulse (originally chirped from 65 fs) will be further broadened to ~100 fs. The effective thickness of the water layer (that is, the water immersion layer plus the thickness of the tissue) is essentially independent of the imaging depth, making the pulse width approximately constant over the entire imaging depth.

**Imaging setup.** Imaging was performed with a multiphoton microscope[11,12] (Supplementary Fig. S2). We used heavy water ($D_2O$, which is safe and widely available) instead of regular water as the immersion liquid in order to minimize the absorption of the 1,675 nm excitation by the liquid between the objective and the sample surface. The immersion $D_2O$ was sealed from moisture in the air because $D_2O$ is hygroscopic. We used a photomultiplier tube (PMT) with a GaAsP photocathode (H7422-40, quantum efficiency (QE) at 600 nm, ~36%, Hamamatsu Photonics) to detect the fluorescence from Texas Red or RFP tdimer2(12). The filters were a 593 nm long-pass filter (Semrock) and a 630±46 nm bandpass filter (Chroma Technology), respectively, for Texas Red and RFP tdimer2(12). The THG signal (558 nm) was detected through a 558±10 nm bandpass filter (Semrock) by an ultra bialkali PMT (R7600-200, QE at 560 nm, ~10%, Hamamatsu Photonics). A movable objective microscope head (MOM, Sutter Instrument Company) translated the objective axially to change the imaging depth within the sample. The field of view (FOV) for each image was 123 μm × 123 μm. A computer running the ScanImage[29] module with MATLAB (Mathworks) software controlled translation of the objective and image acquisition. Current generated by the PMT was converted to voltage (0.1 V $\mu A^{-1}$) and low-pass-filtered (20 kHz) by a transimpedance amplifier (C7319, Hamamatsu Photonics). Analog-to-digital conversion was performed by a data acquisition card (NI PCI-6110, National Instruments) at a sampling rate up to 5 million samples per second. Owing to the low repetition rate of the laser (1 MHz), the pixel clock was ~15 μs, resulting in oversampling by our data acquisition card. For depth measurement, the slightly larger index of refraction in brain tissue (1.35–1.4 for the cortex[30,31] and as high as 1.467 for the white matter[31]), relative to water (~1.33), resulted in a slight underestimate (5–10%) of the actual imaging depth within the tissue, because the imaging depths reported here are the raw axial movement of the objective. For image processing, a median filter with a one-pixel radius was applied.

For *in vivo* axial resolution measurements, we drew a line across the capillary vessels in the fast scanning direction, and measured the maximum brightness along this line at each depth to obtain the axial brightness profile. This approach partially mitigated the motion artefacts caused by heartbeat and breathing, and avoided the dark pixels inside the capillary vessel caused by non-labelled blood cells.

**Animal procedures.** Animal procedures were reviewed and approved by the Cornell Institutional Animal Care and Use Committee. We used male FVB/N mice (23 g, 10 weeks old, Charles River) for Texas Red-labelled vasculature imaging, and B6.Cg-Tg(Thy1-Brainbow1.0)HLich/J mice (18 g, 6 weeks old, The Jackson Laboratory) for RFP-labelled neuron imaging. Animals were prepared using the methods described by Kobat[12]; craniotomies were performed centred at 2 mm posterior and 2 mm lateral to the Bregma point. Before imaging the FVB/N mice, 200 μl of 70 kDa Texas Red–dextran (Invitrogen, dissolved at 5% wt/vol in saline) was retro-orbitally injected to label the vasculature. The B6.Cg-Tg(Thy1-Brainbow1.0)HLich/J mice were not subjected to Cre recombinase, so the only fluorescent protein expression was from RFP tdimer2(12).

**Perfusion and slicing.** Mice (B6.Cg-Tg(Thy1-Brainbow1.0)HLich/J) were killed and perfused. Brain slices were prepared and imaged using the post-mortem histology methods described by Rosidi[32].

Received 13 June 2012; accepted 3 December 2012; published online 20 January 2013

## References

1. Denk, W., Strickler, J. H. & Webb, W. W. Two-photon laser scanning fluorescence microscopy. *Science* **248,** 73–76 (1990).
2. Kerr, J. N. D. & Denk, W. Imaging *in vivo*: watching the brain in action. *Nature Rev. Neurosci.* **9,** 195–205 (2008).
3. Dombeck, D. A., Harvey, C. D., Tian, L., Looger, L. L. & Tank, D. W. Functional imaging of hippocampal place cells at cellular resolution during virtual navigation. *Nature Neurosci.* **13,** 1433–1440 (2010).
4. Olivier, N. *et al.* Cell lineage reconstruction of early zebrafish embryos using label-free nonlinear microscopy. *Science* **329,** 967–971 (2010).
5. Williams, R. M. *et al.* Strategies for high-resolution imaging of epithelial ovarian cancer by laparoscopic nonlinear microscopy. *Trans. Oncol.* **3,** 181–194 (2010).
6. Jung, J. C., Mehta, A. D., Aksay, E., Stepnoski, R. & Schnitzer, M. J. *In vivo* mammalian brain imaging using one- and two-photon fluorescence microendoscopy. *J. Neurophysiol.* **92,** 3121–3133 (2004).

7. Levene, M. J., Dombeck, D. A., Kasischke, K. A., Molloy, R. P. & Webb, W. W. *In vivo* multiphoton microscopy of deep brain tissue. *J. Neurophysiol.* **91,** 1908–1912 (2004).
8. Kleinfeld, D., Mitra, P. P., Helmchen, F. & Denk, W. Fluctuations and stimulus induced changes in blood flow observed in individual capillaries in layers 2 through 4 of rat neocortex. *Proc. Natl Acad. Sci. USA* **95,** 15741–15746 (1998).
9. Svoboda, K., Helmchen, F., Denk, W. & Tank, D. W. Spread of dendritic excitation in layer 2/3 pyramidal neurons in rat barrel cortex in vivo. *Nature Neurosci.* **2,** 65–73 (1999).
10. Theer, P., Hasan, M. T. & Denk, W. Two-photon imaging to a depth of 1000 μm in living brains by use of a Ti:$Al_2O_3$ regenerative amplifier. *Opt. Lett.* **28,** 1022–1024 (2003).
11. Kobat, D. *et al.* Deep tissue multiphoton microscopy using longer wavelength excitation. *Opt. Express* **17,** 13354–13364 (2009).
12. Kobat, D., Horton, N. G. & Xu, C. *In vivo* two-photon microscopy to 1.6-mm depth in mouse cortex. *J. Biomed. Opt.* **16,** 106014 (2011).
13. Helmchen, F. & Denk, W. Deep tissue two-photon microscopy. *Nature Methods* **2,** 932–940 (2005).
14. Balu, M. *et al.* Effect of excitation wavelength on penetration depth in nonlinear optical microscopy of turbid media. *J. Biomed. Opt.* **14,** 010508 (2009).
15. Sacks, Z. S., Kurtz, R., Juhasz, T., Spooner, G. & Mouroua, G. A. Subsurface photodisruption in human sclera: wavelength dependence. *Ophthalmic Surg. Lasers Imag.* **34,** 104–113 (2003).
16. Kou, L., Labrie, D. & Chylek, P. Refractive indices of water and ice in the 0.65- to 2.5-μm spectral range. *Appl. Opt.* **32,** 3531–3540 (1993).
17. Xu, C., Zipfel, W., Shear, J. B., Williams, R. M. & Webb, W. W. Multiphoton fluorescence excitation: new spectral windows for biological nonlinear microscopy. *Proc. Natl Acad. Sci. USA* **93,** 10763–10768 (1996).
18. Hell, S. W. *et al.* Three-photon excitation in fluorescence microscopy. *J. Biomed. Opt.* **1,** 71–74 (1996).
19. Wokosin, D. L., Centonze, V. E., Crittenden, S. & White, J. Three-photon excitation fluorescence imaging of biological specimens using an all-solid-state laser. *Bioimaging* **4,** 208–214 (1996).
20. Zysset, B., Beaud, P. & Hodel, W. Generation of optical solitons in the wavelength region 1.37–1.49 μm. *Appl. Phys. Lett.* **50,** 1027–1029 (1987).
21. Wang, K. & Xu, C. Tunable high-energy soliton pulse generation from a large-mode-area fiber and its application to third harmonic generation microscopy. *Appl. Phys. Lett.* **99,** 071112 (2011).
22. Limpert, J. *et al.* High-power rod-type photonic crystal fiber laser. *Opt. Express* **13,** 1055–1058 (2005).
23. Barad, Y., Eisenberg, H., Horowitz, M. & Silberberg, Y. Nonlinear scanning laser microscopy by third harmonic generation. *Appl. Phys. Lett.* **70,** 922–924 (1997).
24. Müller, M., Squier, J., Wilson, K. R. & Brakenhoff, G. J. 3D microscopy of transparent objects using third-harmonic generation. *J. Microsc.* **191,** 266–274 (1998).
25. Farrar, M. J., Wise, F. W., Fetcho, J. R. & Schaffer, C. B. *In vivo* imaging of myelin in the vertebrate central nervous system using third harmonic generation microscopy. *Biophys. J.* **100,** 1362–1371 (2011).
26. Livet, J. *et al.* Transgenic strategies for combinatorial expression of fluorescent proteins in the nervous system. *Nature* **450,** 56–62 (2007).
27. Franklin, K. B. J. & Paxinos, G. *Mouse Brain in Stereotaxic Coordinates* (Academic Press, 2008).
28. Murphy, P. A *et al.* Notch4 normalization reduces blood vessel size in arteriovenous malformations. *Sci. Transl. Med.* **4,** 117ra8 (2012).
29. Pologruto, T. A., Sabatini, B. L. & Svoboda, K. ScanImage: flexible software for operating laser scanning microscopes. *Biomed. Eng. Online* **2,** 13 (2003).
30. Binding, J. *et al.* Brain refractive index measured in vivo with high-NA defocus corrected full-field OCT and consequences for two-photon microscopy. *Opt. Express* **19,** 4833–4847 (2011).
31. Bacallao, R., Sohrab, S. & Phillips, C. in *Handbook of Biological Confocal Microscopy* (ed. Pawley, J. B.) 368–380 (Springer, 2006).
32. Rosidi, N. L. *et al.* Cortical microhemorrhages cause local inflammation but do not trigger widespread dendrite degeneration. *PLoS ONE* **6,** e26612 (2011).


## Acknowledgements

This work is partially funded by grants from the National Institutes of Health (NIH; R01CA133148, R01EB014873 and R21RR032392). N.G.H. is supported by the National Science Foundation Graduate Research Fellowship Program (DGE-0707428). The authors acknowledge discussions with D. Dombeck, as well as N. Nishimura and J. Rubin, regarding preparation of the *ex vivo* brain slices.

## Author contributions

C.X. initiated and supervised the study. N.G.H., K.W., D.K. and C.G.C. performed the experiments and data analysis. N.G.H., K.W., D.K. and C.X. contributed to the writing and editing of the manuscript. C.B.S. and C.X. contributed to the design of the experiments. F.W. and C.X. contributed to the laser source design.

## Additional information

Supplementary information is available in the online version of the paper. Reprints and permission information is available online at http://www.nature.com/reprints. Correspondence and requests for materials should be addressed to C.X.

## Competing financial interests

The authors declare no competing financial interests.